Chapter 3:
Compound defect in Black Phosphorene

3.1 Introduction

Defect engineering offers a highly effective avenue for tailoring the physical and chemical attributes of materials. Point defects such as dopants, vacancies, and interstitials are broadly known for their ability to modify the physiochemical properties of two-dimensional (2D) materials, providing distinct advantages over their pristine counterparts in specific applications. For instance, doping with light non-metallic elements such as B, N, O, and F can significantly influence the structural and electronic properties of graphene [1]. Beyond graphene, doping foreign elements into other 2D materials, such as *h*-BN, WS_2, and WSe_2, has also been shown to effectively tailor their structural, electronic, optical, and functional properties [2–4]. Another point defect which prominently influences the aforementioned properties of 2D materials is vacancy. Vacancies can be generated both extrinsically and intrinsically, leading to structural deformation at the atomic scale. This disrupts the orbital hybridization of the pristine system, causing these modifications.

In this chapter, special attention has been given to the study of formation and stability of a compound defect in black phosphorene (BP), and the influence of the defect on its structural and electronic properties. Here, we define a 'compound defect' as the simultaneous presence of two different point defects within the system. BP is a p-type semiconductor with an electronic band gap of 0.90 eV - 1.00 eV [5]. Notably, it exhibits anisotropic electrical conductance, high chemical reactivity, and exceptionally high hole mobility (reaching up to 1000 $cm^2V^{-1}s^{-1}$ at room temperature). Given its attractive properties, pristine BP has found widespread applications in electronics, nanosensors, and beyond [6–9]. However, despite such intriguing and attractive properties, BP has a poor structural stability in the ambient environment and is susceptible to defects, particularly vacancies (refer to Table 1.1) [10]. As a result, there is always a very high possibility that a BP structure doped with a foreign element will also possess phosphorous (P) vacancies within it. This gives rise to the novel concept of compound defect.

To date, only a few studies on 2D materials have considered the presence and influence of compound defects, despite reports indicating significant modifications in structural and electronic properties [2,11]. The compound defect considered in this study incorporates a nitrogen (N) doped BP system with the combination of P vacancy. Nitrogen is chosen as the dopant due to its high binding energy with BP, reducing the likelihood of

structural degradation upon doping [12]. First principles calculation is employed to study the structural and chemical stability of the compound defect. Furthermore, we examine the changes in the electronic properties of the monolayer with the compound defect under uniaxial strain ranging from -5% to 5%.

3.2 Model and computational details

3.3.1 DFT parameters

The calculations were carried out via first principles using density functional theory (DFT), a plane wave basis set, as implemented in QUANTUM ESPRESSO [13]. Projector-augmented waves (PAWs) pseudo potentials within a dense Monkhorst *k*-grid of 6×1×6 and 12×1×12 was used for the self-consistent field and non-self-consistent field calculations, respectively [14–16]. Perdew-Burke-Ernzerhof (PBE) exchange-correlation functional with generalised gradient approximation (GGA) was considered for all the calculations [17]. The values of kinetic energy cutoff and charge density were set to 50 Ry and 300 Ry, respectively. The structures were allowed to relax until a force convergence threshold of 10^{-3} Ry/Bohr was achieved. The convergence criteria for the self-consistent calculations were chosen to be 10^{-6} Ry for all the modelled structures.

3.2.2 Structural modelling

The calculated lattice parameters of BP monolayer along the armchair (ac) and zigzag (zz) direction are 4.47 Å and 3.33 Å. This is consistent with the previous reports [18]. Based on the optimised parameters of the monolayer unit cell, a 3×3 supercell is modelled to introduce the defects into BP (Fig. 3.1(a,b)). To eradicate the interactions between the interlayers, a vacuum of 15 Å is added to the atomic plane in the perpendicular direction. The sp^3 hybridised BP, having each P atom bonded to other three P atoms, leaving a lone pair of electrons, forms a puckered layer structure. The puckered structural nature of BP makes the monolayer atomically two layer thin (Fig. 3.1(b)). The BP system with a single P vacancy is shown in Fig. 3.1(c), and N doped BP is shown in Fig. 3.1(d). To model the compound defect in the monolayer, first, we create a P vacancy in the upper atomic layer of the monolayer BP. Then we add the dopant N atom in different atomic sites. Due to the puckered two-layer atomic structure, the compound point defect can exist in four possible configurations in the monolayer. **(a)** Both P vacancy and N dopant can reside near one another in the same atomic layer (Fig. 3.2(a): N atom is doped adjacent to the

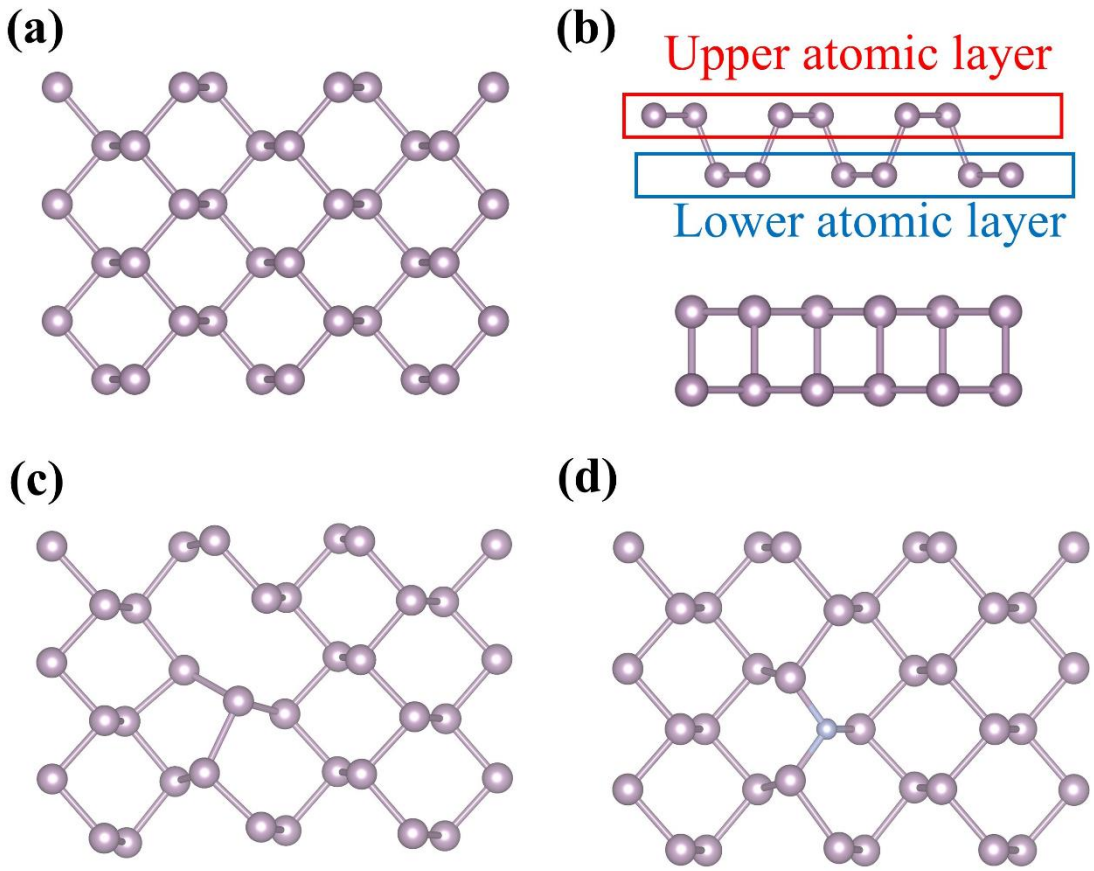

Figure 3.1: *(a) Top view, and (b) side view of 3×3 supercell of pristine BP; (c) BP with a P vacancy (BP_V), and (d) BP with a doped N atom (BP^N).*

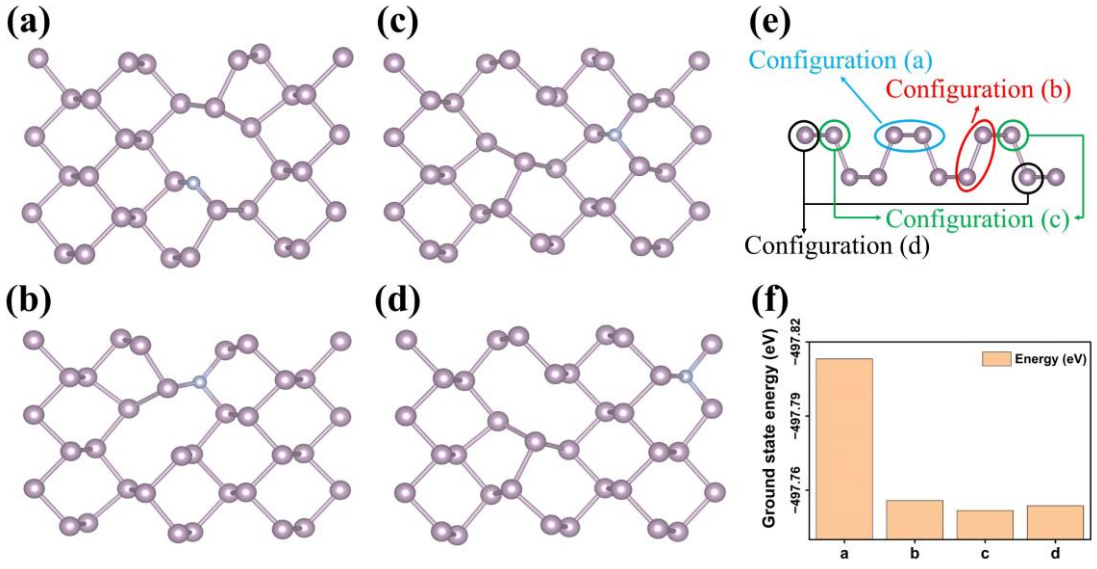

Figure 3.2: *(a-d) Four different configurations of compound defect in BP; (e) side view (along ac direction) of the four possible configurations of the compound defect in BP; (f) ground state energy of the four configurations.*

vacant site in the upper atomic layer), **(b)** Both P vacancy and N dopant can reside close to one another in the different atomic layer (Fig. 3.2(b): N atom is doped adjacent to the vacant site in the lower atomic layer), **(c)** Both P vacancy and N dopant can reside away from one another in the same atomic layer (Fig. 3.2(c): N atom is doped away from the vacant site in the upper atomic layer), and **(d)** Both P vacancy and N dopant can reside away from one another in the different atomic layer (Fig. 3.2(d): N atom is doped away from the vacant site in the lower atomic layer). A schematic depiction of the four configurations from the side view is shown in Fig. 3.2(e). To obtain the configuration with the highest stability, we compare the ground state energy of the four configurations (Fig. 3.2(f)). It is evident that when the N is doped in the upper atomic layer right next to the vacant site, the structure has the lowest ground state energy, ensuring the configuration to be most stable among the four (Fig. 3.2(a)).

3.3 Stability of compound defect

At first, we compute the formation energy of a P vacancy within pristine BP using the following formula:

$$E_{vf} = E_{BP_v} - N_P \times E_P \quad \ldots(3.1)$$

where, E_{BP_v} denotes the total ground state energy of BP with a vacancy, E_P represents the energy per P atom in pristine BP, and N_P signifies the number of phosphorene atoms in the monolayer. It should be noted that the E_{vf} value for pristine BP is 0 eV. The formation energy of BP_v is found to be 1.51 eV, consistent with the earlier report [5]. Compared to other 2D materials such as graphene (7.80 eV), silicene (3.77 eV), TMDCs like WSe_2 (5.30 eV for W, 2.63 eV for Se), as well as TMMCs such as SnS (4.75 eV for Sn), 6.03 eV for S), the energy required to create a P vacancy in BP is significantly lower [4,5,19].

The formation energy of two P vacancies in BP is calculated by modifying the equation (3.1) into the following form:

$$E_{vf} = E_{BP_{2v}} - N_P \times E_P \quad \ldots(3.2)$$

$E_{BP_{2v}}$ is the ground state energy of BP system containing two P vacancies. The energy required to form two P vacancies is 1.56 eV. In comparison, the divacancy formation energy in graphene and silicene is 7.52 eV and 3.70 eV, respectively. This indicates that

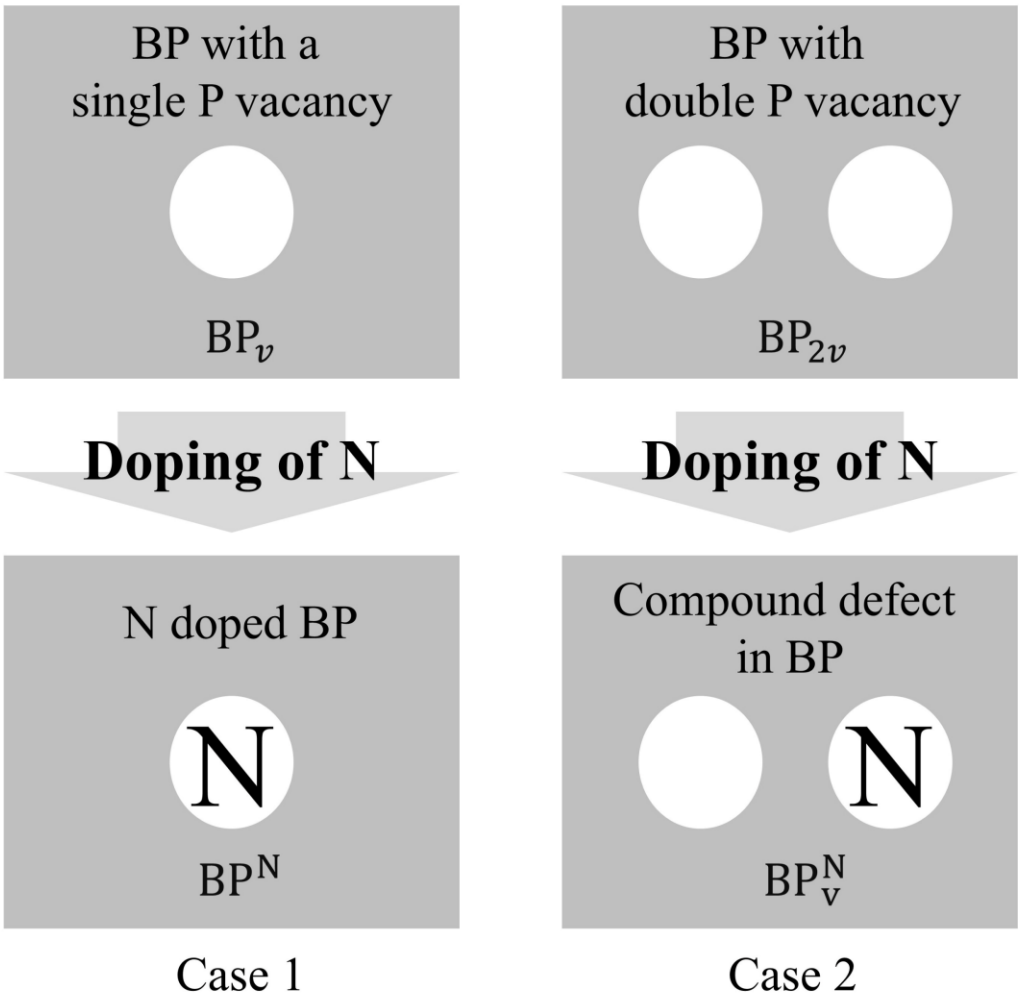

Figure 3.3: *Schematic depicting the formation of compound defect in BP.*

vacancies in BP can form much more easily, making them an almost inevitable feature of the system.

Next, we calculate the binding energy of the doped N atom in the two BP monolayers. Two doping scenarios are considered: (case 1) the N atom binds to a BP system with a single P vacancy (BP_v), or (case 2) the N atom binds to a BP system with two P vacancies (BP^N) (as illustrated in Fig. 3.3). Notably, a compound defect can form only if the second scenario is energetically more favourable. The binding energy for BP^N monolayer is calculated using the following formula:

$$E_b = E_{BP_v} + E_N - E_{BP^N} \quad \ldots(3.3)$$

where, E_{BP_v}, and E_{BP^N} represent the total ground state energies of the BP monolayer with a single vacancy (i.e., BP_v) and BP^N monolayers, respectively; the term E_N represents the

energy of the dopant N. To obtain the B.E of BP_v^N, equation (3.3) is modified into the following form:

$$E_b = E_{BP_{2v}} + E_N - E_{BP_v^N} \quad \ldots(3.4)$$

here, $E_{BP_{2v}}$ is the total ground state energy of a BP monolayer with two P vacancies, and the term $E_{BP_v^N}$ represents the total ground energy of BP_v^N monolayer. The B.E energies of N in BP^N and BP_v^N monolayer is obtained to be 5.65 eV and 5.04 eV, respectively. This shows that the doped N atom is more likely to reside with a P vacancy in BP monolayer, forming a compound defect.

In addition, the chemical stability of the pristine BP, BP_v, BP^N, and BP_v^N monolayers are checked by calculating the cohesive energy (E_c) using the following formula:

$$E_c = \frac{E_{(BP/BP_v/BP^N/BP_v^N)} - \sum_i n_i E(i)}{\sum_i n_i} \quad \ldots(3.5)$$

here, n_i represents the number of atoms 'i' in the system, and the energy of the isolated atoms are represented by $E(i)$.

The cohesive energies for the pristine BP, BP_v, BP^N, and BP_v^N systems are found to be -3.42 eV, -3.38 eV, -3.44 eV, and -3.43 eV, respectively. The marginal disparities in the E_c values among the BP_v, BP^N, and BP_v^N systems compared to pristine BP indicate that vacancies or doping exert minimal effect on the chemical stability of the pristine system.

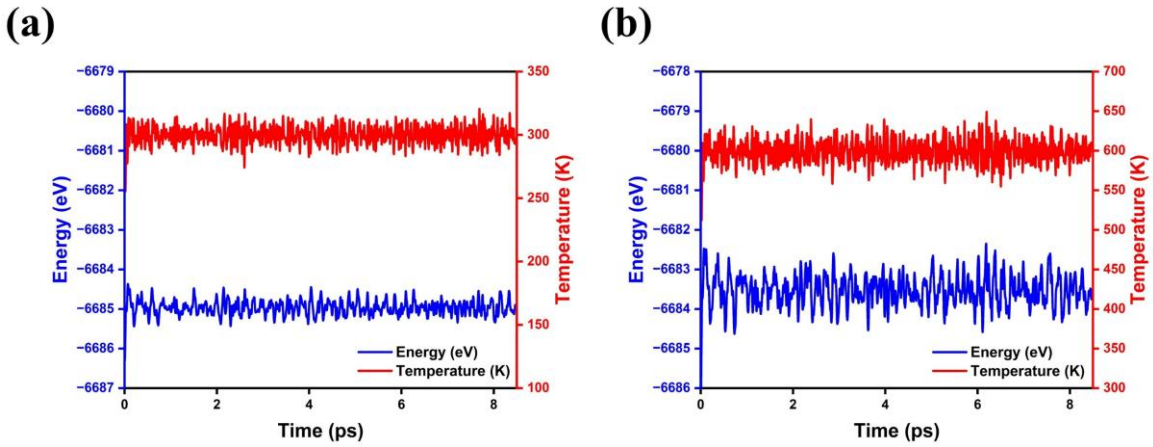

Figure 3.4: *AIMD simulation of BP_v^N at (a) 300 K and (b) 600 K over a time period of 8.5 ps (the axis on the left side of the figures represents the energy of the heterostructure and the axis on the right side of the figures represents the temperature scale).*

Additionally, the E_c value of BP_v^N closely aligns with that of pristine BP, indicating the negligible compromise to the chemical stability of the pristine system by the compound defect, in contrast to systems with a single-point defect.

Furthermore, *ab initio* molecular dynamics (AIMD) simulations were carried out at 300 K (room temperature) and 600 K to assess the thermal stability of the BP_v^N system (Fig. 3.4). The energy fluctuations at these two temperatures were compared with the binding energy of the compound defect. The minimal fluctuations over a time period of 8.5 ps indicate to the thermal stability of BP_v^N up to 600 K.

3.4 Electronic properties

The electronic band structure and projected density of states (PDOS) of pristine BP, BP_v, BP^N, and BP_v^N are shown in Fig. 3.5, and Fig. 3.6, respectively. At DFT-GGA level, pristine BP is a nonmagnetic material and exhibits a direct band gap of 0.78 eV at the Γ point of the BZ (Fig. 3.5(a)). This result is in agreement with the earlier report [5]. When a P vacancy is introduced into the BP monolayer, the valence band intersects the Fermi level, indicating the injection of holes into the system (Fig. 3.5(b)). Additionally, as shown in Fig. 3.5(b), the vacancy induces a symmetrical disparity between the spin-up and spin-down states in the valence band, resulting in a magnetic moment of 0.84 μ_B within the system. The structural deformation originating from the vacant site in the monolayer leads to significant changes in the P-P bond lengths in its vicinity. Consequently, the outer shell electrons give rise to asymmetric states near the Fermi level, thereby instigating magnetism in the monolayer. The PDOS (Fig. 3.6(b)) clearly indicates that this asymmetry originates from the *2p* orbital of the P atom. The results for BP_v are in agreement with the earlier reports [5].

When an N atom substitutes for a P atom in the BP monolayer, the system remains nonmagnetic. This is because N and P hold analogous electronic configurations and correspond to the identical group in the periodic table. However, the doped N atom affects the electronic band structure of BP, increasing it to 0.86 eV (Fig. 3.5(c)). Nevertheless, the nature of the gap remains direct at the Γ point of the BZ, reflecting similarities with pristine BP.

Upon combining both the point defects in the monolayer BP, the valence band along the X-Γ direction exhibits an almost flat band-like behaviour. As illustrated in Fig. 3.5(d), the

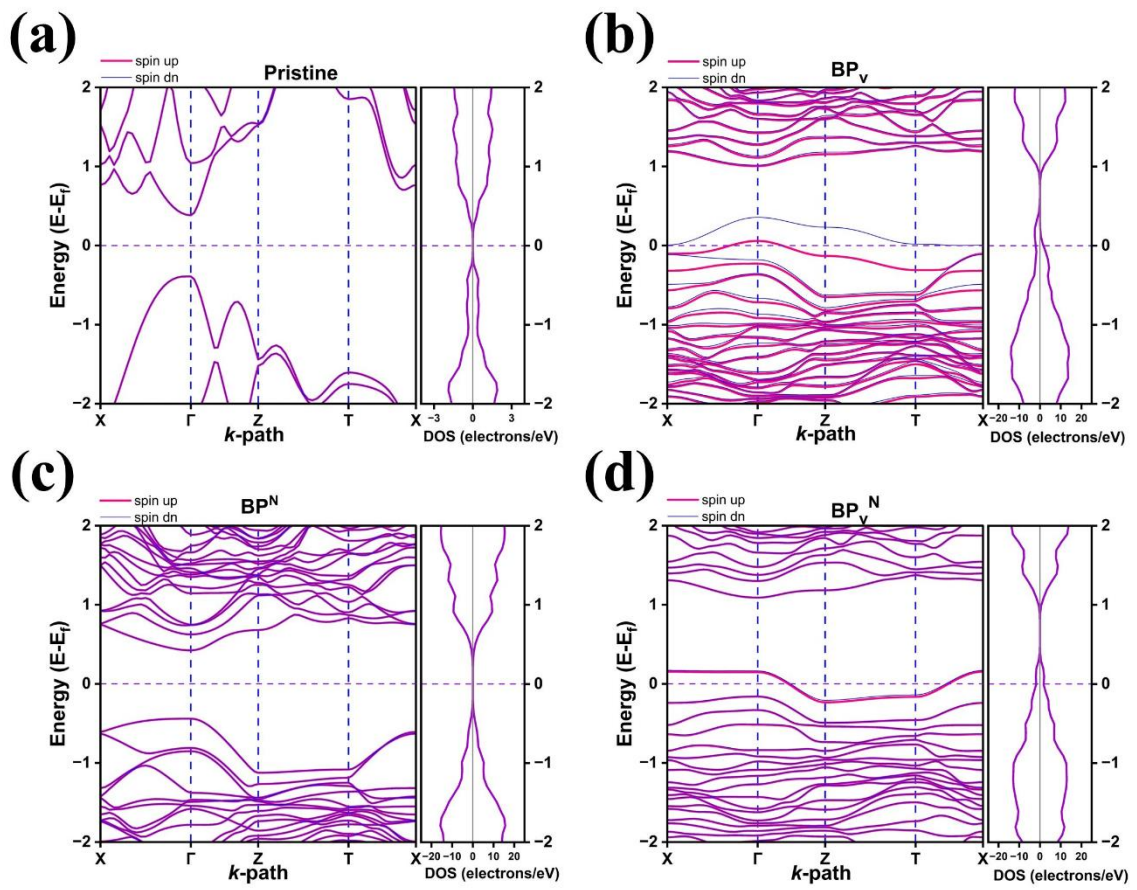

Figure 3.5: *Electronic band structure (spin up and spin down bands are indicated by pink and blue colours, respectively) and DOS plots of (a) pristine BP, (b) BP^N, (c) BP_v, and (d) BP_v^N system (energy scale is in eV).*

dispersive nature of the valence band along the X-Γ direction nearly vanishes. This suggests a very low hole mobility in the monolayer BP_v^N. The flat nature of the valence band gives rise to an indirect band gap in the monolayer along the X-Γ direction, while the direct band gap of the monolayer remains at the Γ point but increases to 0.93 eV from 0.78 eV compared to pristine BP. In fact, the monolayer with a compound point defect now features two competing band gaps of 0.92 eV (indirect, along X-Γ) and 0.93 eV (direct). Similar to the BP_v monolayer, the presence of a vacancy also increases the hole concentration in the BP_v^N monolayer as the Fermi level crosses the valence band. However, the presence of the N atom in the vicinity of the vacant site compensates for the magnetism produced by the vacancy, indicating the monolayer with a compound defect to be almost nonmagnetic. The magnetic moment of BP_v^N monolayer is obtained to be 0.10 μ_B.

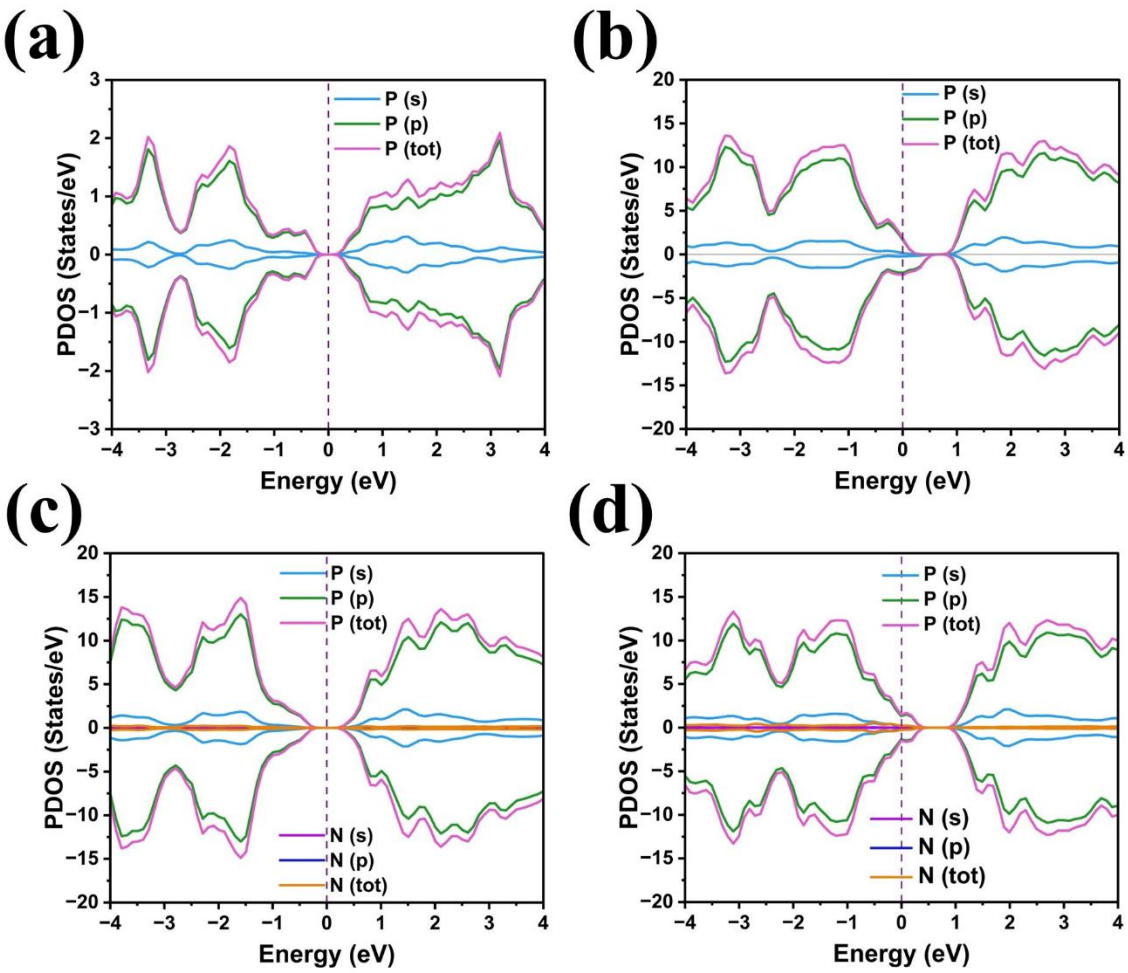

Figure 3.6: *PDOS of (a) pristine BP, (b) BP^N, (c) BP_v, and (d) BP_v^N system.*

3.5 Effect of strain

Table 3.1: Lattice parameters of the 3×3 BP_v^N supercell under different uniaxial strain along the zz and ac direction.

Strain %	zigzag		armchair	
	a (Å)	c (Å)	a (Å)	c (Å)
no strain (0%)	10.00	13.42	10.00	13.42
1 %	10.10	13.42	10.00	13.56
3 %	10.30	13.42	10.00	13.82
5 %	10.50	13.42	10.00	14.09
-1 %	9.90	13.42	10.00	13.29
-3 %	9.70	13.42	10.00	13.02
-5 %	9.50	13.42	10.00	12.75

Moving forward, we explore the impact of tensile and compressive uniaxial strain along the zz and ac directions of BP_v^N to study the alterations in the electronic and magnetic properties of the system with a compound point defect. The applied strain is estimated using the formula given by:

$$\text{strain } (\%) = \frac{L_s - L_c}{L_c} \times 100 \qquad \ldots(3.6)$$

where, L_c is the lattice parameter of the 3×3 cell, and L_s is the lattice parameter of the supercell under strain. The negative sign of strain percentage indicates to a compressive strain, and the positive sign indicates to a tensile strain on the system. The lattice parameters of BP_v^N under the uniaxial strains are shown in Table 3.1.

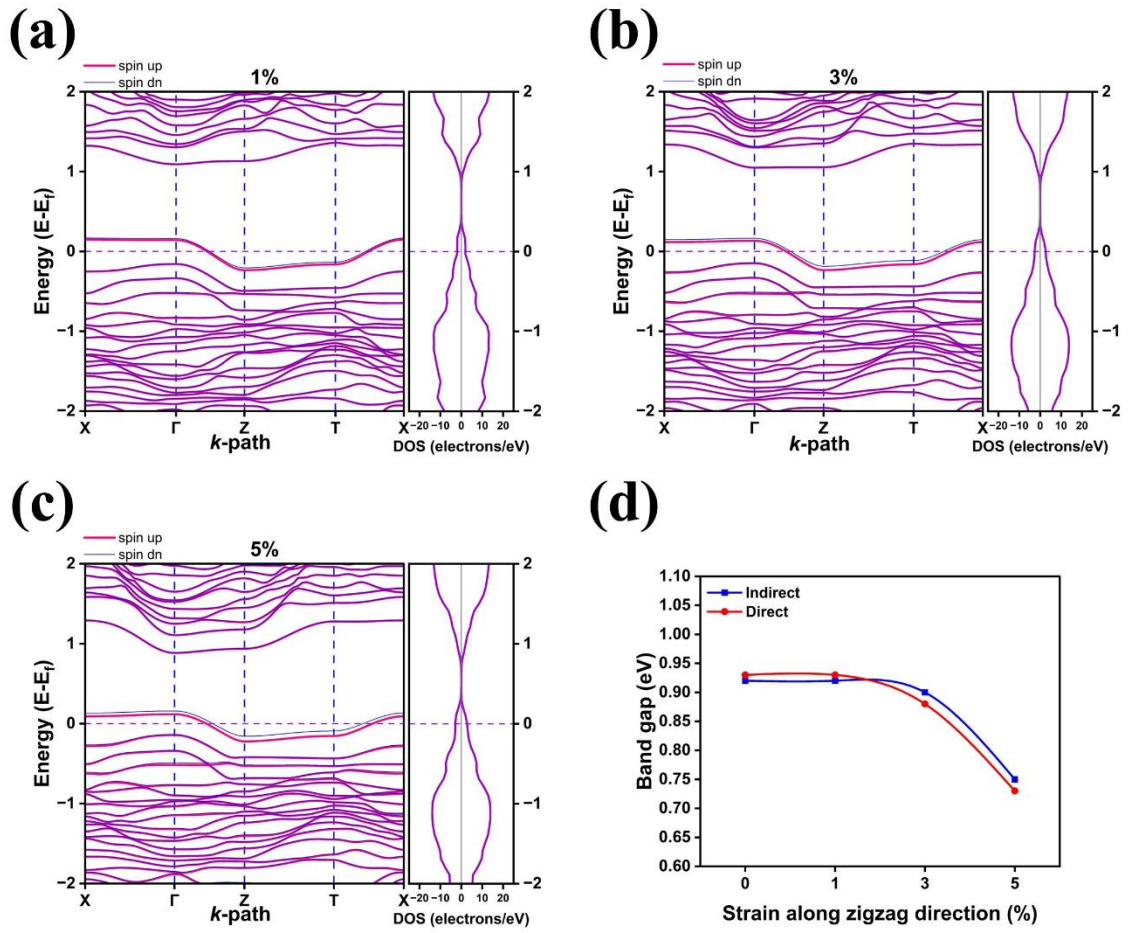

Figure 3.7: *Band structure of BP_v^N monolayer under (a) 1% strain, (b) 3% strain, (c) 5% strain along the zz direction, respectively; (d) band gap values of BP_v^N under tensile along the zz direction; (spin up and spin down bands are indicated by pink and blue colours, respectively) (energy scale is in eV).*

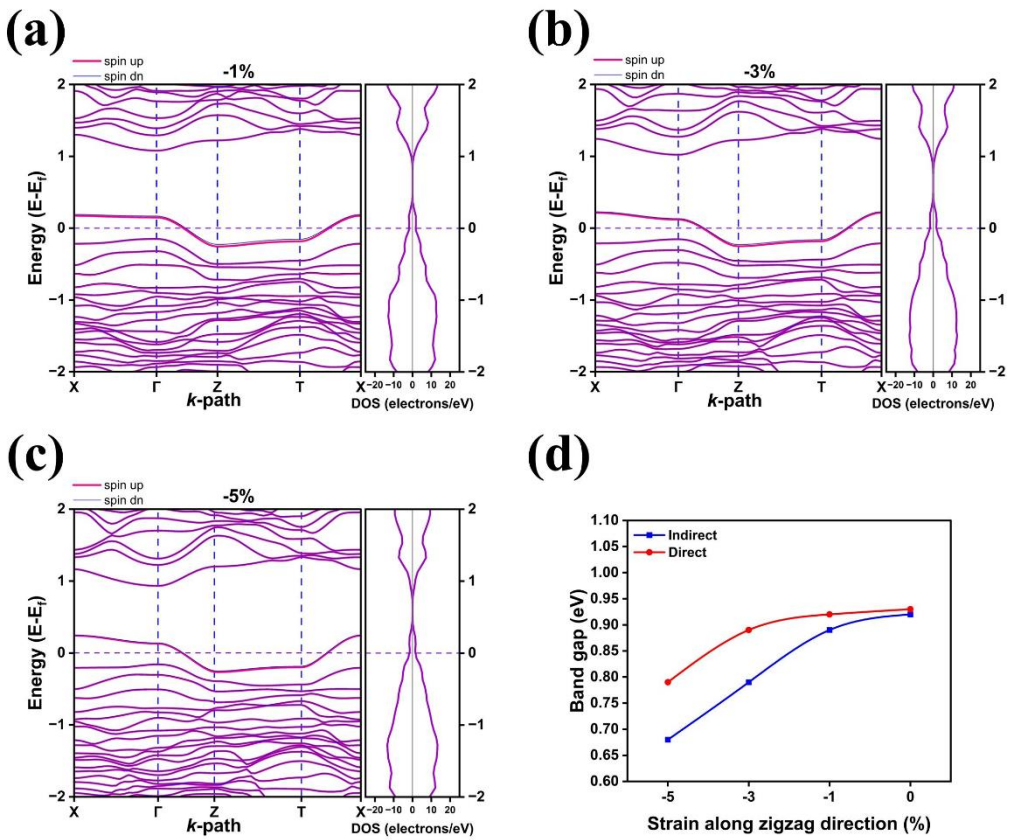

Figure 3.8: *Band structure of BP_v^N monolayer under (a) -1% strain, (b) -3% strain, (c) -5% strain along the zz direction, respectively; (d) band gap values of BP_v^N under compressive along the zz direction; (spin up and spin down bands are indicated by pink and blue colours, respectively) (energy scale is in eV).*

Table 3.2: Band gaps and magnetic moments of BP_v^N monolayer under tensile and compressive strain along zz direction.

Strain (%)	Band gap (eV)		Magnetic moment (μ_B)
	X-Γ (indirect)	Γ-Γ (direct)	
0	0.92	0.93	0.10
1	0.92	0.93	0.12
3	0.90	0.88	0.19
5	0.75	0.73	0.24
-1	0.89	0.92	0.13
-3	0.79	0.89	0.11
-5	0.68	0.79	0.10

Upon applying 1%, 3%, and 5% tensile strain along the zz direction of BP_v^N monolayer, the electronic band gap starts decreasing gradually (Table 3.2 and Fig. 3.7). The indirect and direct band gap of BP_v^N drops down to 0.75 eV and 0.73 eV, respectively, under the tensile strain of 5%. The nature of the change of band gap under compressive strain along the zz direction also remains the same and gradually decreases to 0.68 eV (indirect) and 0.79 eV (direct) under -5% strain (Table 3.2 and Fig. 3.8). From Table 3.2, it can be seen that there is a slight increase in the magnetic moment of BP_v^N monolayer as the tensile strain increases, but is almost negligible as the splitting of spin up and down states in the electronic band structure is not prominent (Fig. 3.7 and Fig. 3.8). The values of magnetic moment remain unchanged under compressive strain along the zz direction.

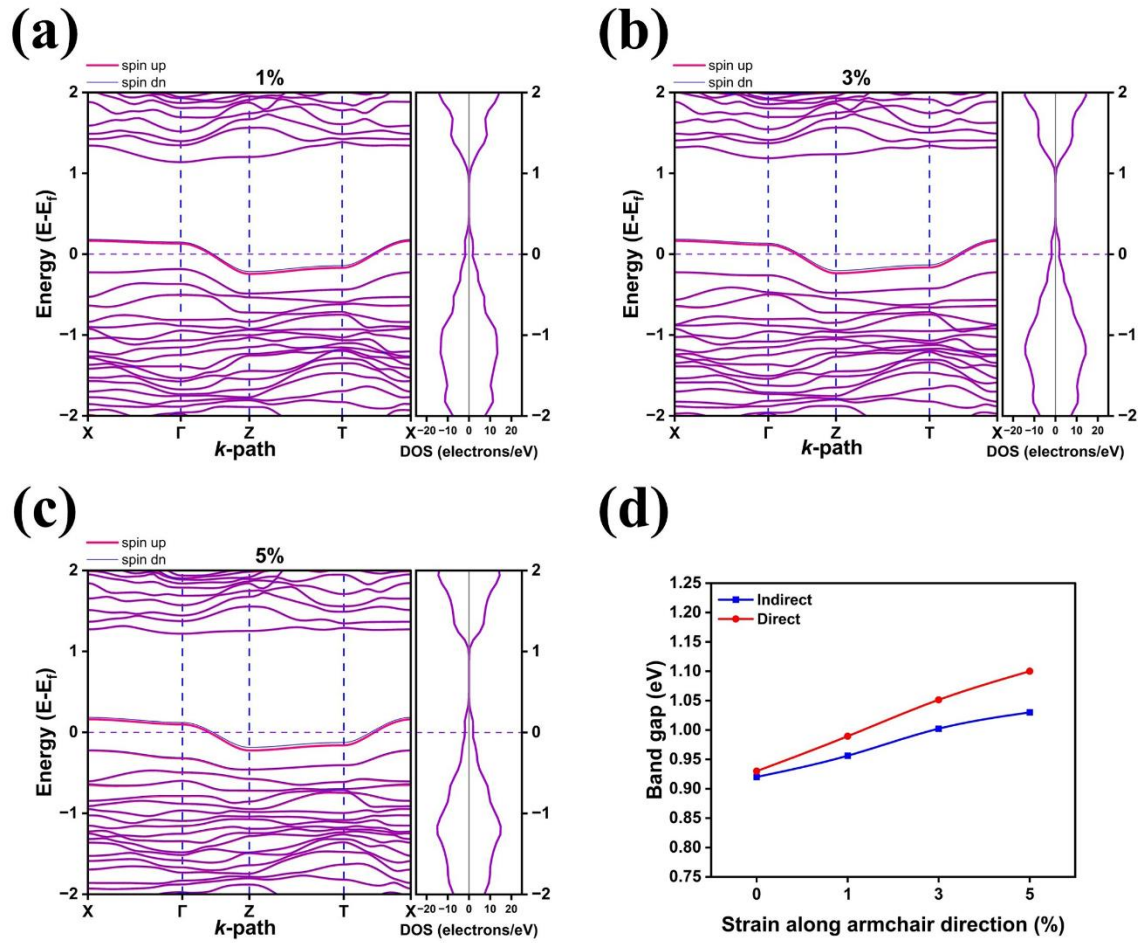

Figure 3.9: *Band structure of BP_v^N monolayer under (a) 1% strain, (b) 3% strain, (c) 5% strain along the ac direction, respectively; (d) band gap values of BP_v^N under tensile along the ac direction; (spin up and spin down bands are indicated by pink and blue colours, respectively) (energy scale is in eV).*

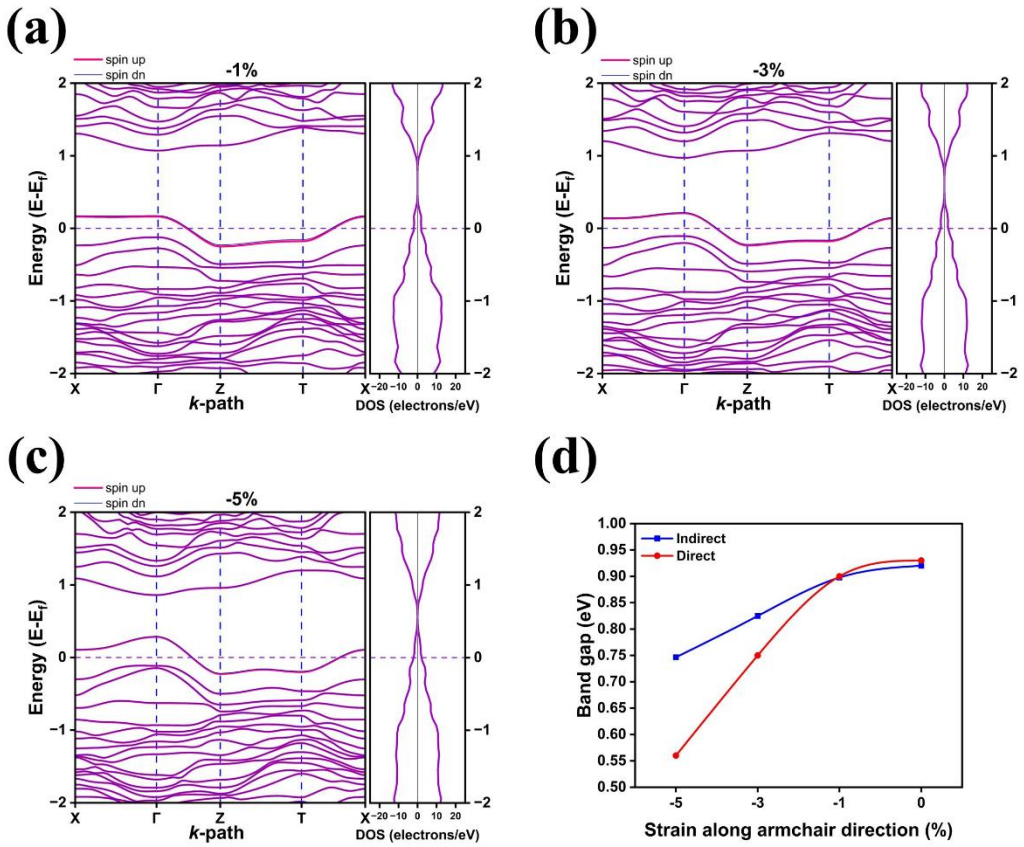

Figure 3.10: *Band structure of BP_v^N monolayer under (a) -1% strain, (b) -3% strain, (c) -5% strain along the ac direction, respectively; (d) band gap values of BP_v^N under compressive along the ac direction; (spin up and spin down bands are indicated by pink and blue colours, respectively) (energy scale is in eV).*

Table 3.3: Band gaps and magnetic moments of BP_v^N monolayer under tensile and compressive strain along ac direction.

Strain (%)	Band gap (eV)		Magnetic moment (μ_B)
	X-Γ (indirect)	Γ-Γ (direct)	
0	0.92	0.93	0.10
1	0.96	0.99	0.12
3	1.00	1.05	0.13
5	1.03	1.10	0.13
-1	0.90	0.90	0.11
-3	0.82	0.75	0.07
-5	0.75	0.57	0.05

The band gap of BP_V^N under compressive strain along the ac direction also shows a similar nature to that of zz direction. At a maximum strain of -5%, the indirect (direct) band gap of the system decreases to 0.75 eV (0.57 eV) (Table 3.3 and Fig. 3.9). The magnetic moment of the system starts reducing as the compressive strain increases. In contrast, under tensile strain along the ac direction, the band gap of BP_V^N start increasing as the strain increases. The maximum indirect (direct) band gap of BP_V^N under 5% strain is 1.03 eV (1.10 eV) (Table 3.3 and Fig. 3.10). The magnetic moment for the tensile strain along ac remains almost constant with the increase in strain.

3.6 Conclusion

In conclusion, first principles calculations have been employed to study the structural, chemical, and thermal stability of BP monolayer with a compound defect. The vacancy formation energy of 1.51 eV suggests that the vacancies can be easily formed in a pristine BP system. In addition, the lower binding energy of N in BP_V^N as compared to BP^N monolayer suggests that the doped atom is more likely to form a compound defect in pristine BP with the simultaneous presence of a P vacancy. The least deviating cohesive energy of the BP_V^N system from pristine BP also indicates to a very strong chemical stability of the system. These results indicate N is more favourable to be doped in BP_V monolayer than in pristine BP monolayer, forming a compound defect in the system. Furthermore, electronic nature of BP_V^N monolayer under uniaxial strain in the zz and ac direction have also been investigated. Our results reveal that under both compressive and tensile strain along the zz direction, the band gap of the BP_V^N monolayer decreases as the strain increases. The indirect (direct) band gap of BP_V^N drops to 0.68 eV (0.79 eV), and 0.75 eV (0.73 eV) under the highest compressive and tensile strain in the zz direction, respectively. Interestingly, along the ac direction, the indirect (direct) band gap of BP_V^N monolayer decreases with increase in compressive strain to 0.75 eV (0.57 eV), but increases with tensile strain to 1.03 eV (1.10 eV). These variations in band gap arise from structural changes in the system under strain. The lattice parameters of the BP unit cell with a vacancy BP_V^N experience notable changes under uniaxial compressive or tensile strain along both the ac and zz axes. These lattice parameter changes affect the P-P bond lengths and bond angles, modifying the sp^3 orbital hybridization of BP. Notably, the BP monolayer with compound defects in our study retains the anisotropic response of pristine BP under strain, demonstrating a similar sensitivity to directional strain.

The presence of compound defects, combined with the inherent anisotropic structural and electronic properties of BP, can significantly alter its surface functionalities. This opens up an avenue for BP_V^N to exhibit enhanced surface adsorption properties, making it an exceptional candidate for next-generation nanosensing devices. The role of compound defects in sensing different toxic gas molecules are discussed in detail in the next chapter.

References

[1] Wu, M., Cao, C., Jiang, J. Z. Light non-metallic atom (B, N, O and F)-doped graphene: a first-principles study. *Nanotechnology*, 21(50): 505202, 2010.

[2] Deka, B., Talukdar, D., Naik, V., Saha, A., Mohanta, D. Generating immiscible localized WC phase in layered WS_2 upon 15 keV C^{2+} irradiation. *Physica Scripta*, 100(2): 025931, 2025.

[3] Talukdar, D., Bora, S. S., Ahmed, G. A. Electronic, optical, and adsorption properties of Li-doped hexagonal boron nitride: a GW approach. *Physical Chemistry Chemical Physics*, 26(5): 4021–4028, 2024.

[4] Deka, B., Talukdar, D., Mohanta, D. Effect of 60 MeV nitrogen ion irradiation on few layer WSe_2 nanosystems. *Nuclear Instruments and Methods in Physics Research Section B: Beam Interactions with Materials and Atoms*, 554: 165438, 2024.

[5] Hu, W., Yang, J. Defects in phosphorene. *The Journal of Physical Chemistry C*, 119(35): 20474–20480, 2015.

[6] Kumar, A., Viscardi, L., Faella, E., Giubileo, F., Intonti, K., Pelella, A., Sleziona, S., Kharsah, O., Schleberger, M. and Di Bartolomeo, A. Temperature dependent black phosphorus transistor and memory. *Nano Express*, 4(1): 014001, 2023.

[7] Ding, K., Wen, L., Huang, S., Li, Y., Zhang, Y., Lu, Y. Electronic properties of red and black phosphorous and their potential application as photocatalysts. *RSC advances*, 6(84): 80872–80884, 2016.

[8] Zhang, H., Zhang, R., Sun, C., Jiao, Y., Zhang, Y. CO_2 reduction to CH_4 on Cu-doped phosphorene: a first-principles study. *Nanoscale*, 13(48): 20541–20549, 2021.

[9] Zhang, H., Du, A., Shi, Q., Zhou, Y., Zhang, Y., Tang, Y. Adsorption behavior of CO_2 on pristine and doped phosphorenes: A dispersion corrected DFT study. *Journal of CO_2 Utilization*, 24: 463–470, 2018.

[10] Kistanov, A. A., Cai, Y., Zhou, K., Dmitriev, S. V, Zhang, Y. W. The role of H_2O and O_2 molecules and phosphorus vacancies in the structure instability of phosphorene. *2D Materials*, 4(1): 015010, 2016.

[11] Fartab, D. S., Kordbacheh, A. A. Lithium doping and vacancy effects on the structural, electronic and magnetic properties of hexagonal boron nitride sheet: A first-principles calculation. *Superlattices and Microstructures*, 118: 185–195, 2018.

[12] Yang, L., Mi, W., Wang, X. Tailoring magnetism of black phosphorene doped with B, C, N, O, F, S and Se atom: a DFT calculation. *Journal of Alloys and Compounds*, 662: 528–533, 2016.

[13] Giannozzi, P., Baroni, S., Bonini, N., Calandra, M., Car, R., Cavazzoni, C., Ceresoli, D., Chiarotti, G.L., Cococcioni, M., Dabo, I., Dal Corso, A. QUANTUM ESPRESSO: a modular and open-source software project for quantum simulations of materials. *Journal of physics: Condensed matter*, 21(39): 395502, 2009.

[14] Holzwarth, N. A. W., Tackett, A. R., Matthews, G. E. A Projector Augmented Wave (PAW) code for electronic structure calculations, Part I: atompaw for generating atom-centered functions. *Computer Physics Communications*, 135(3): 329–347, 2001.

[15] Kresse, G., Joubert, D. From ultrasoft pseudopotentials to the projector augmented-wave method. *Physical review b*, 59(3): 1758, 1999.

[16] Monkhorst, H. J., Pack, J. D. Special points for Brillouin-zone integrations. *Physical review B*, 13(12): 5188, 1976.

[17] Perdew, J. P., Burke, K., Ernzerhof, M. Generalized gradient approximation made simple. *Physical review letters*, 77(18): 3865, 1996.

[18] Luan, Z., Zhao, L., Chang, H., Sun, D., Tan, C., Huang, Y. First-principles study on electronic structures and magnetic properties of Eu-doped phosphorene. *Superlattices and Microstructures*, 111: 816–823, 2017.

[19] Ullah, H., Kim, H. J., Shin, Y. H. Influences of vacancy and doping on electronic and magnetic properties of monolayer SnS. *Journal of Applied Physics*, 124(6): 2018.